TECHNISCHE MECHANIK, Band 23, Heft 2-4, (2003), 160– 166
Manuskripteingang: 14. Juli 2003

Dynamic Strain Aging, Negative Strain-Rate Sensitivity and Related Instabilities

A. Benallal, T. Borvik, A. Clausen, O. Hopperstad

We give in this paper a possible mechanical interpretation to the development of Lüders front and Portevin-Le-Chatelier effect based on a band analysis for an elastic- viscoplastic material with negative strain-rate sensitivity. This negative strain rate sensitivity allows for jumps for the plastic strain rate which in turns permits the existence of localization bands for the elastic-viscoplastic material. The classical band analysis for an infinite solid does not predict the direction of the band. However, we show that this direction is determined in some circumstances if one considers the boundary conditions.

1 Introduction

Lüders fronts and Portevin-Le-Chatelier (PLC) effect are widely observed phenomena. Both phenomena are usually associated to dynamic strain aging, i.e. the dynamic interaction between mobile dislocations and solute atoms (Kubin and Estrin, 1985). Dynamic strain aging occurs for temperatures and strain-rates within a certain range, but sometimes a critical strain is required for serrated yielding to take place. A widely accepted consequence of dynamic strain aging is the negative strain rate sensitivity that is observed for many alloys. The propagation of deformation bands associated with the Portevin-Le-Chatelier effect may occur in a continuous or discontinuous manner. The initiation of each band is evidenced by a yield point on the stress-time curve which is followed by a relatively smooth curve during band propagation, see e.g. McCormick et al. (1993). The main result of this paper is to explain the appearance of such bands for an elastic-viscoplastic material if one includes negative strain-rate sensitivity and to compute the orientation of these bands by considering the boundary conditions. The study is completed by a linear perturbation approach to highlight the effects of the negative strain-rate sensitivity on the behaviour of the material. The critical condition for the growth of perturbations is linked to the condition of the appearance of the Lüders fronts and PLC effect.

2 Constitutive Equations with Negative Strain-Rate Sensitivity

2.1 Experimental Observations

An experimental program has been carried out on axisymmetric specimens made of the aluminium alloy AA5083. This alloy shows anisotropic characteristics. However, the longitudinal axis of all specimens is parallel with the rolling direction. Both quasi-static and dynamic uniaxial tensile tests were performed. The tests are carried out at room temperature and strain-rates between 10^{-4} and $10^{3}s^{-1}$. The tests with strain rates up to approximately $10s^{-1}$ were carried out on an Instron tension machine with digital control electronics. A Split-Hopkinson tension bar (SHTB) was employed for the tests with strain rates larger than $10^{2}s^{-1}$. The axisymmetric samples were machined from 10 mm thick rolled plates. Figure 1 shows true stress versus plastic strain curves for four selected tests with distinctly different strain rates. It is interesting to note that the highest strength is obtained by the quasistatic strain rate of $0.00041s^{-1}$. The two curves associated with the intermediate strain rates are lower, thereby indicating a negative strain rate effect. At the highest strain rate of $1313s^{-1}$, however, the strength shows an increasing tendency. The curves in Figure 1 are interrupted at the ultimate strain, where necking occurs. This strain, and accordingly the ductility, increases considerabely as function of strain rate. It is beyond the scope of this paper to discuss this phenomenon more thoroughly, but the effect is undoubtedly real, as the fracture strains, which can be checked after each test, also increase with strain rate. The flow stress at a plastic strain of 5 percent, denoted here $\boldsymbol{\sigma}_5$, is chosen as the parameter describing the strain rate sensitivity. Figure 2 shows the observed $\boldsymbol{\sigma}_5$

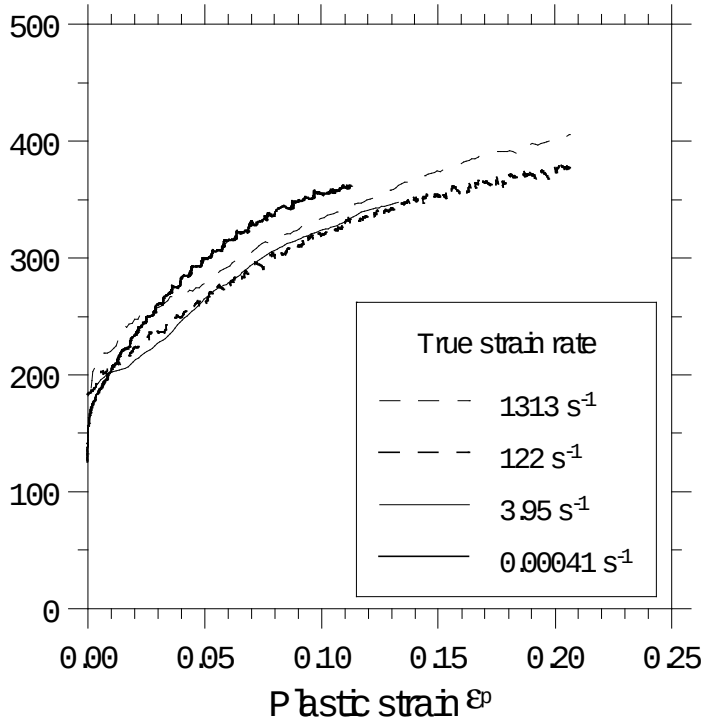

Figure 1: Stress-strain curves for Aluminium Alloy AA 5083 at different strain rates.

as function of strain rate. The four circular points refer to the tests presented in Figure 1. The upper abscissa axis in Figure 2 is consistent with the common way of representing strain rates by using the logarithm function with base 10, while the lower abscissa axis is associated with a dimensionless strain rate. Although some scatter is present,

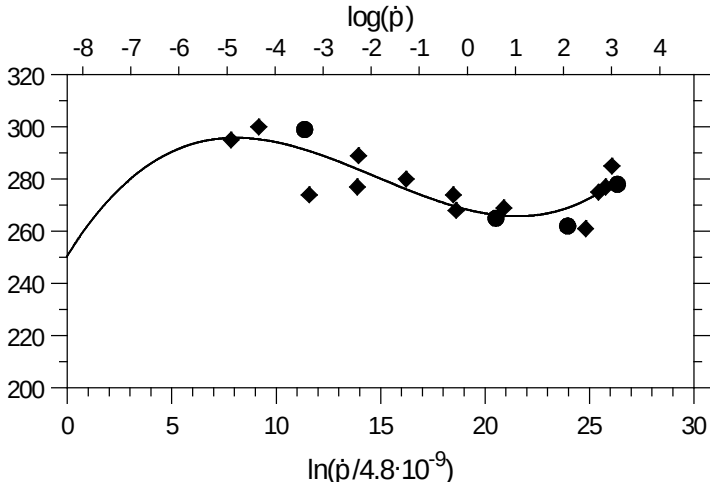

Figure 2: Flow stress $\boldsymbol{\sigma}_5$ as a function of strain rate.

the flow stress seems to have a significant drop when the strain rate increases from $10^{-4}s^{-1}$ to $10s^{-1}$. Thereafter, $\boldsymbol{\sigma}_5$ ascends until $10^3 s^{-1}$, which is the maximum attainable strain rate in the SHTB situated at SIMLab. It is interesting to note that there is a rather good agreement between the $\boldsymbol{\sigma}_5$ observations at $5s^{-1}$, which are obtained with the Instron machine, and the Split Hopkinson Tension Bar flow stress at $100s^{-1}$.

2.2 General Framework

To interpret these phenomena, we consider in this paper an elastic-viscoplastic material the behaviour of which involves negative strain rate sensitivity. The behavior of the material is determined first by the free energy potential

$\Psi(\boldsymbol{\epsilon}, \boldsymbol{\alpha})$ depending on the strain tensor $\boldsymbol{\epsilon}$ and a set of internal variables $\boldsymbol{\alpha}$ assumed to describe various physical mechanisms. The knowledge of the free energy potential leads to the state laws defining the Cauchy stress tensor $\boldsymbol{\sigma}$ and the thermodynamical forces $\mathbf{A}$ associated to the internal variables $\boldsymbol{\alpha}$ as

$$\boldsymbol{\sigma} = \rho \frac{\partial \Psi}{\partial \boldsymbol{\epsilon}}, \text{ and } \mathbf{A} = -\rho \frac{\partial \Psi}{\partial \boldsymbol{\alpha}} \tag{1}$$

where ρ is the mass density. The evolution of the internal variables is defined by a reversibility domain C (inside which no irreversibility occurs), the equation of which in the forces space is $f(\mathbf{A}, \boldsymbol{\alpha}) < 0$ and by a flow potential $F(\mathbf{A}, \boldsymbol{\alpha})$ such that

$$\dot{\boldsymbol{\alpha}} = \dot{p} \frac{\partial F}{\partial \mathbf{A}} \text{ with } \dot{p} = \frac{1}{\mu} < \Phi'(f) > \tag{2}$$

In (2) and for classical viscoplasticity, $\Phi'(f)$ is an increasing positive function of f satisfying $\Phi'(f) > 0$, μ a positive constant, and $< x >= Max(x, 0)$. The ' denotes the derivative with respect to f. In this paper, to describe negative strain rate sensitivity, we consider the simple following model

$$\dot{p} = \frac{1}{\mu(\dot{p})} < \Phi'(f) > \tag{3}$$

in such a way that the equation

$$\dot{p}\mu(\dot{p}) = \Phi'(f) \tag{4}$$

has many solutions and describes experimental data shown in figure 2. These experimental results actually suggest three solutions. In the above formula and in the whole paper, the dot denotes the material time rate. Moreover the functions Ψ, F, f and Φ are chosen so that the Clausius-Duhem inequality expressing the second law be satisfied.

2.3 An Example

As an accompagning example in this paper we will consider the following simple constitutive relations. One tensorial internal variable $\boldsymbol{\epsilon}^p$ (plastic strain) and one scalar internal variable p (accumulated plastic strain) are introduced to describe inelastic behaviour with isotropic hardening. The free energy, the plastic potential and the yield function are

$$\Psi(\boldsymbol{\epsilon}, \boldsymbol{\epsilon}^p, p) = \frac{1}{2}(\boldsymbol{\epsilon} - \boldsymbol{\epsilon}^p) : \mathbf{E} : (\boldsymbol{\epsilon} - \boldsymbol{\epsilon}^p) + w(p) \tag{5}$$

$$f = F = J_2(\boldsymbol{\sigma}) - R - \sigma_e \tag{6}$$

where $J_2(\boldsymbol{\sigma}) = \sqrt{\frac{3}{2}\mathbf{s} : \mathbf{s}}$. $\mathbf{s}$ is the stress deviator, $\mathbf{E}$ is elasticity tensor, R the force associated to p and σ_e the initial yield stress. The function $\Phi = \frac{K}{2}(\frac{f}{K})^2$ is considered.

3 Band Analysis

3.1 Infinite Space

We perform in this section a band analysis. This is very classical in the context of strain localisation for rate-independent materials. For classical elastic-viscoplastic materials jumps on the strain rate are ruled out (at least in the small strain regime). We show below that these jumps may emerge if the elastic-viscplastic material exhibits negative strain rate sensitivity. An infinite homogeneous body that is homogeneously deformed is considered. We seek for the conditions under which a bifurcation from this homogeneous state with strain rate $\dot{\boldsymbol{\epsilon}}_0$ to a heteregeneous one including a band of normal $\mathbf{n}$ with strain rate $\dot{\boldsymbol{\epsilon}}_1$ becomes possible, the strain rate outside the band being still $\dot{\boldsymbol{\epsilon}}_0$. The Maxwell kinematic compatibility relations imply that

$$\dot{\boldsymbol{\epsilon}}_1 - \dot{\boldsymbol{\epsilon}}_0 = \frac{1}{2}[\mathbf{g} \otimes \mathbf{n} + \mathbf{n} \otimes \mathbf{g}] \tag{7}$$

The rate form of constitutive equations lead outside and inside the band, respectively, to

$$\dot{\boldsymbol{\sigma}}_0 = \mathbf{E} : \dot{\boldsymbol{\epsilon}}_0 - \dot{p}_0 \mathbf{E} : \frac{\partial f}{\partial \boldsymbol{\sigma}} \tag{8}$$

$$\dot{\boldsymbol{\sigma}}_1 = \mathbf{E} : \dot{\boldsymbol{\epsilon}}_1 - \dot{p}_1 \mathbf{E} : \frac{\partial f}{\partial \boldsymbol{\sigma}} \tag{9}$$

Continuuing equilibrium across the band gives

$$\dot{\boldsymbol{\sigma}}_1 . \mathbf{n} = \dot{\boldsymbol{\sigma}}_0 . \mathbf{n} \tag{10}$$

Using (7) , (8) and (9) in (10), one has

$$(\mathbf{n}.\mathbf{E}.\mathbf{n}).g - (\dot{p}_1 - \dot{p}_0)\mathbf{E} : \frac{\partial f}{\partial \boldsymbol{\sigma}} = 0 \tag{11}$$

To obtain relation (11), it was assumed that the state of the material is the same outside and inside the band. At this stage, with classical viscoplasticity and no negative strain rate sensitivity, $\dot{p}_1 = \dot{p}_0$ and no jumps in the plastic nor in the total strain rates is possible. In presence of both positive and negative strain rate sensitivity in the material behaviour, it is possible under some circumstances that for a fixed given state (as the one prevailing outside and inside the band for instance) that different accumulated plastic strain rates are possible for this state. This indeed happens for instance at such points in Figure 2 where the ¤ow stress passes trough a maximum or a minimum. One may choose any of these inside the band that is different from $\dot{p}_0$. In this case, the searched bifurcation mode exists and one has from (11),

$$\mathbf{g} = (\dot{p}_1 - \dot{p}_0)[\mathbf{n}.\mathbf{E}.\mathbf{n}]^{-1}.(\mathbf{n}.\mathbf{E} : \frac{\partial f}{\partial \boldsymbol{\sigma}}) \tag{12}$$

The difference $\dot{p}_1 - \dot{p}_0$ is obtained through the constitutive equations and particularly from (4) with f depending on the state (i.e. stress, hardening parameters, etc....). For a given state, relation (4) has only a *finite number* of solutions in terms of $\dot{p}$ as seen from experimental data depicted in figure 2. The following conclusions hold

- For a given jump $\dot{p}_1 - \dot{p}_0$ and for a given orientation $\mathbf{n}$, the amplitude $\mathbf{g}$ is unique.
- From (11), the normal $\mathbf{n}$ to the band is unspecified.
- At each jump in the plastic strain rate, there is a jump in the total strain rate except in the directions $\mathbf{n}$ such that $\mathbf{n}.\mathbf{E} : \frac{\partial f}{\partial \boldsymbol{\sigma}} = 0$.
- The mode described above will exist only when the constitutive relations allow for a multiple solution for the plastic strain rate. This mode will appear only in the associated regime, see e.g. Figure 2.

3.2 Band Orientation

We have mentioned in the former section that the normal $\mathbf{n}$ was arbitray. We will show here that this arbitrariness is removed when one considers boundary conditions. The simplest way to do so is to reformulate the band analysis carried out before for a homogeneous and homogeneously deformed half-space. We will come back later to the practical case of a finite specimen. We denote by $\mathbf{m}$ the unit outward normal to this half-space and keep all the notations similar to the one adopted for the infinite space. We seek now conditions for the same mode to emerge. All the reasoning followed in the former section is still valid. We just need to include the boundary conditions. Different types of such conditions may be considered: displacement or velocity conditions, traction conditions and all the combinations between these two types. Let us analyse here the most common situation of a free surface where the traction vector should vanish

$$\boldsymbol{\sigma}.\mathbf{m} = 0 \tag{13}$$

Two conditions have to be met for the band to meet the boundary. These are easily written respectively outside and inside the band (using the notations of the infinite space) as

$$\dot{\boldsymbol{\sigma}}_0.\mathbf{m} = 0 \tag{14}$$

$$\dot{\boldsymbol{\sigma}}_1.\mathbf{m} = 0 \tag{15}$$

Taking the difference of these two equations, using the constitutive equations and taking into account (7) we have

$$\dot{\boldsymbol{\sigma}}_1.\mathbf{m} - \dot{\boldsymbol{\sigma}}_0.\mathbf{m} = [\mathbf{m}.\mathbf{E}.\mathbf{n}].\mathbf{g} - (\dot{p}_1 - \dot{p}_0)\mathbf{m}.\mathbf{E} : \frac{\partial f}{\partial \boldsymbol{\sigma}} = 0 \tag{16}$$

Using the expression (12) of $\mathbf{g}$ in this last equation one gets in the case where $\dot{p}_1 - \dot{p}_0 \neq 0$

$$[\mathbf{m}.\mathbf{E}.\mathbf{n}].[\mathbf{n}.\mathbf{E}.\mathbf{n}]^{-1}.(\mathbf{n}.\mathbf{E} : \frac{\partial f}{\partial \boldsymbol{\sigma}}) - \mathbf{m}.\mathbf{E} : \frac{\partial f}{\partial \boldsymbol{\sigma}} = 0 \tag{17}$$

This equation sets now a constraint in the normal to the band at least in the vicinity of the boundary. Indeed one may imagine two possiblities: the band may have the same orientation all along or may have a given orientation in the bulk of the material and then kinks at the vicinity of the boundary. We exploit this condition for isotropic elasticity. We denote by λ and G the Lame coefficients so that

$$E_{ijkl} = \lambda\delta_{ij}\delta_{kl} + G(\delta_{ik}\delta_{jl} + \delta_{il}\delta_{jk}) \tag{18}$$

Bands will be available when equation (17) admits real solutions $\mathbf{n}$.

The critical condition will be analysed in the principal frame $(\mathbf{e}_1, \mathbf{e}_2, \mathbf{e}_3)$ of the flow direction $\mathbf{a} = \frac{\partial f}{\partial \boldsymbol{\sigma}}$ where we set

$$\mathbf{a} = \{\{a_1, 0, 0\}, \{0, a_2, 0\}, \{0, 0, a_3\}\} \tag{19}$$

and

$$\mathbf{n} = \{n_1, n_2, n_3\}, \mathbf{m} = \{m_1, m_2, m_3\} \tag{20}$$

We have then

$$\mathbf{n}.\mathbf{E}.\mathbf{a} = \{\lambda\ (a_1 + 2\,a_2)\ n_1 + 2\,G\,n_1, \lambda\ (a_1 + 2\,a_2)\ n_2 + 2\,G\,n_2, \lambda\ (a_1 + 2\,a_2)\ n_3 + 2\,G\,n_3\} \tag{21}$$

$$\mathbf{m}.\mathbf{E}.\mathbf{a} = \{\lambda\ (a_1 + 2\,a_2)\ m_1 + 2\,G\,m_1, \lambda\ (a_1 + 2\,a_2)\ m_2 + 2\,G\,m_2, \lambda\ (a_1 + 2\,a_2)\ m_3 + 2\,G\,m_3\} \tag{22}$$

$$\mathbf{n}.\mathbf{E}.\mathbf{n} = \begin{bmatrix} G + (G+\lambda)\,n_1^2 & (G+\lambda)\,n_1\,n_2 & (G+\lambda)\ n_1\,n_3 \\ (G+\lambda)\ n_1 n_2 & G + (G+\lambda)\,n_2^2 & (G+\lambda)\,n_2\,n_3 \\ (G+\lambda)\ n_1 n_3 & (G+\lambda)\,n_2\,n_3 & G + (G+\lambda)\ n_3^2 \end{bmatrix} \tag{23}$$

3.3 Application to the Tension Test

From now on, we will consider tension tests in the $\mathbf{e}_3$ direction. In this case, assuming J_2 plasticity, we have $\mathbf{a} = \mathbf{s}$ where $\mathbf{s}$ is the stress deviator and $a_1 = a_2 = -\frac{a_3}{2}$. In these conditions, the critical condition (17) takes the form

$$\begin{array}{c} m_1\ \left(2\,G + \lambda - \lambda n_2^2 + 2\,\lambda n_3^2 + n_1^2\ \left(-2\,G - \lambda - 6\ (G+\lambda)\,n_3^2\right)\right) \\ +n_1\ \left(2\,m_2\,n_2\ \left(-G - 3\ (G+\lambda)\ n_3^2\right) + m_3\,n_3\ \left(G + 3\ (G+\lambda)\ \left(n_1^2 + n_2^2 - n_3^2\right)\right)\right) = 0 \end{array} \tag{24}$$

$$\begin{array}{c} m_2\ \left(2\,G + \lambda - \lambda n_1^2 + 2\,\lambda\,n_3^2 - n_2^2\ \left(2\,G + \lambda + 6\ (G+\lambda)\,n_3^2\right)\right) \\ +n_2\ \left(2\,m_1\,n_1\ \left(-G - 3\ (G+\lambda)\,n_3^2\right) + m_3\,n_3\ \left(G + 3\ (G+\lambda)\ \left(n_1^2 + n_2^2 - n_3^2\right)\right)\right) = 0 \end{array} \tag{25}$$

$$\begin{array}{c} -\left(m_3\ \left(4\,G + 2\,\lambda + \lambda n_1^2 + \lambda n_2^2\right)\right) + 2\,m_3\ \left(2\,G + \lambda + 3\ (G+\lambda)\ \left(n_1^2 + n_2^2\right)\right)\ n_3^2 \\ +\left(m_1\,n_1 + m_2\,n_2\right)\ n_3\ \left(G + 3\ (G+\lambda)\ \left(n_1^2 + n_2^2 - n_3^2\right)\right) = 0 \end{array} \tag{26}$$

In the following we consider two different specimens: a flat one and a cylindrical one, both with axis $\mathbf{e}_3$, the tension axis.

3.3.1 Solutions in the Case of a Cylindrical Specimen

In the case of the round specimen, one can work on the associated cylindrical coordinates so that

$$\mathbf{e}_1 = \mathbf{e}_r, \mathbf{e}_2 = \mathbf{e}_\theta, \mathbf{e}_3 = \mathbf{e}_z \tag{27}$$

We therefore have at any boundary point of the specimen $\mathbf{m} = \mathbf{e}_r$ and one has to satisfy

$$2\,G + \lambda + 2\,\lambda n_3^2 + \left(-2\,G - \lambda - 6\ (G+\lambda)\,n_3^2\right)\,n_r^2 - \lambda n_\theta^2 = 0 \tag{28}$$

$$\left(-G - 3\ (G+\lambda)\,n_3^2\right)\ n_r\,n_\theta = 0 \tag{29}$$

$$n_3\,n_r\ \left(G + 3\ (G+\lambda)\ \left(-n_3^2 + n_r^2 + n_\theta^2\right)\right) = 0 \tag{30}$$

- Equations (29) and (30) are both satisfied for $n_r = 0$. This implies that $n_\theta^2 + n_3^2 = 1$ and from (28) one obtains $n_3^2 = -\frac{2G}{3\lambda}$, which is impossible. Therefore $n_r \neq 0$.
- Equation (30) has also $n_3 = 0$ as a solution. But the two other equations cannot be satisfied and $n_3 \neq 0$.
- Equation (29) is satisfied for $n_\theta = 0$. This implies that $n_r^2 + n_3^2 = 1$. Reporting this in (28) and (30) leads to two solutions: either $n_3 = 0$ and therefore $\mathbf{n} = \mathbf{e}_r$ or

$$n_r^2 = \frac{2G + 3\lambda}{6(G + \lambda)} \text{ and therefore } n_3^2 = \frac{4G + 3\lambda}{6(G + \lambda)} \tag{31}$$

The first possibility is of no interest. The second however supports experimental evidence. Indeed experimental observations of band orientation in cylindrical specimens (Wijler (1972), van den Brink (1975), McCormick et al. (1993)) show that the band intersects the surface of the specimen on a plane perpendicular to the tensile axis, and Wijler (1972) proposed that deformation bands in cylindrical specimens are conically shaped. In this case and from (31), the angle θ of this cone is such that (otherwise stated, the band is aligned at an angle θ with the tensile axis)

$$(\tan\theta)^2 = \frac{2G + 3\lambda}{4G + 3\lambda} = \frac{1 + \nu}{2 - \nu} \tag{32}$$

if one introduces Poisson's ratio ν. For a metal $\nu = .30$ and the angle θ is about 53 degrees.

3.3.2 Solutions in the Case of a Flat Specimen

In this case, we have to satisfy the critical conditions at all the sides of the specimen. We therefore have to satisfy condition (17) with $\mathbf{m} = \mathbf{e}_1$ and $\mathbf{m} = \mathbf{e}_2$. Using the above results show that a straight band cannot exist for a three dimensional setting and to comply with the two conditions, the band must kink at the sides of the specimen. In the case of plane situations, the orientation of the band is again given by (31).

4 Perturbation Analysis

In this section a linear perturbation approach is used to show qualitatively the effects of a negative strain-rate sensitivity. A homogeneously deformed body (assumed again infinite here) with uniform properties is considered. At a given stage of its deformation path, an infinitely small perturbation is applied to the solid and the perturbed deformation is analysed. Because the applied perturbation is small, the boundary value-problem (equilibrium and constitutive equations) governing this deformation is linearized around the homogeneous solution. The perturbation fields satisfy then a linear and homogeneous system of partial differential equations. When the perturbations have the form $\delta\mathbf{X} = \tilde{\mathbf{X}} e^{i\xi(\mathbf{n}.\mathbf{x})+\eta t}$ where η is related to the growth of the perturbation), it is shown that the growth condition takes the form

$$\det[\mathbf{n}.\mathbf{H}(\eta).\mathbf{n}] = 0 \tag{33}$$

The general expression of the moduli $\mathbf{H}(\eta)$ can be found in Benallal (2000). For the accompagning model given in section 2, they take the form

$$\mathbf{H}(\eta) = \frac{\eta\sigma_{eq}}{\eta\sigma_{eq} + 3\dot{p}G}\mathbf{E} + \frac{3KG\dot{p}}{\eta\sigma_{eq} + 3\dot{p}G}\mathbf{1}\otimes\mathbf{1} - \frac{9G^2\Big\{\eta[R(p) - \mu^{'}\dot{p}^2] - h\dot{p}\Big\}}{\sigma_{eq}^2(\eta\sigma_{eq} + 3\dot{p}G)[\eta(\mu + \mu^{'}\dot{p}) + h + 3G]}\mathbf{s}\otimes\mathbf{s} \tag{34}$$

Growth of perturbations is signaled by positive values of the real part of the eigenvalues η. If one specializes the analysis to uniaxial conditions the critical condition becomes

$$h + \eta(\mu + \mu^{'}\dot{p}) = 0 \tag{35}$$

from which one can compute the rate of growth of perturbation as

$$\eta = -\frac{h}{\mu + \mu^{'}\dot{p}} = -\frac{h}{\frac{\partial[\mu(\dot{p})\dot{p}]}{\partial\dot{p}}} \tag{36}$$

and allows first insight in the role of negative strain-rate sensitivity ($\frac{\partial[\mu(\dot{p})\dot{p}]}{\partial\dot{p}} < 0$). Indeed, relation (36) shows that for positive strain-rate sentivity ($\frac{\partial[\mu(\dot{p})\dot{p}]}{\partial\dot{p}} > 0$), instabilities are possible only in presence of softening . In the other hand, for negative strain-rate sensitivity, the rate of growth may become positive even in the hardening regime. More importantly, the eigenvalues η may become unbounded (blowing up of perturbations) when the denominator in (36) vanishes, i.e when

$$\mu + \mu^{'}\dot{p} = \frac{\partial[\mu(\dot{p})\dot{p}]}{\partial\dot{p}} = 0 \tag{37}$$

This condition also holds under general three-dimensional conditions. Indeed, the limit of the moduli $\mathbf{H}(\eta)$ in (34) is

$$\lim_{|\eta|\to\infty} \mathbf{H}(\eta) = \begin{cases} \mathbf{E} \text{ if } \mu + \mu^{'}\dot{p} \neq 0 \\ \mathbf{E} - \frac{9G^2[R(\dot{p})-\mu^{'}\dot{p}^2]}{(h+3G)\sigma_{eq}^3}\mathbf{s}\otimes\mathbf{s} \text{ if } \mu + \mu^{'}\dot{p} = 0 \end{cases} \tag{38}$$

5 Conclusions

An interpretation of the appearance of PLC bands has been proposed in the context of elastic-viscoplastic materials with negative strain-rate sensitivity. It allows the determination of the orientation of the bands and the results for axisymmetric specimen seem to support existing conjecture. This is also observed in the finite element simulations of round specimen where conically shaped bands are seen to travel along the gauge length of the specimen.

Acknowledgments

This work was carried out during a stay of A.B. as a visiting Professor at SIM-Lab/NTNU. Financial support and hospitality are gratefully acknowledged. Professor at SIM-Lab/NTNU. Financial support and hospitality are gratefully acknowledged.

References

Benallal, A.: Perturbation and stability of rate-dependent solids. *European Journal of Mechanics A/Solids*, 19, (2000), S45–S60.

Kubin, L.; Estrin, Y.: The portevin-le-chatelier effect in deformation with constant stress rate. *Acta Metallurgica*, 33, (1985), 397–407.

McCormick, P.; Venkadesan, S.; Ling, C.: Propagative instabilities: An experimental view. *Scripta Metallurgica et Materiala*, 29, (1993), 1159–1164.

van den Brink, S.: *Inhomogeneous Deformation in Gold-Copper Alloys*. Ph.D. thesis, Delft (1975).

Wijler, A.: *The Portevin-Le-Chatelier Effect in Gold-Copper Alloys*. Ph.D. thesis, Delft (1972).

Address: Ahmed Benallal, Laboratoire de Mcanique et Technologie, Cachan, France
Tore Borvik, Arild Clausen, Odd-Sture Hopperstad, SIMLab, NTNU, Norway
email: benallal@lmt.ens-cachan.fr; tore.borvik@bygg.ntnu.no
arild.clausen@bygg.ntnu.no;odd.hopperstad@bygg.ntnu.no .